Chapter 4

Central Calorimeter Calibration

The completed central calorimeter has never been in a calibration/test beam. An early effort was made to get a relative calibration between counters from the same ring. The initial calibration involved a Monte Carlo and testing with traversing cosmic ray muons. Part of the calorimeter was tested with electron beams. The calibration of the beam tested counters was transferred to the other counters through the initial relative calibration. The calorimeter's calibration is finely tuned in situ as data is taken. This provides a stack by stack calibration. The calibration and quality of the central calorimeter counter signals are monitored with the gain monitoring system (flashlamp) as well as data.

4.1 Initial Calibration

A Monte Carlo has been developed which predicts the number of photoelectrons produced by a single counter. The Monte Carlo results were combined with the number of photoelectrons and gain curves determined from the PMT tests (section 3.2.1) for initial operating voltages for each counter. The cosmic ray muon tests were then used to initially set the operating voltages for counters from the same ring to have the same response.

4.1.1 Monte Carlo Simulation

A Monte Carlo has been developed to simulate the response of one central calorimeter counter to several different types of incident particles. The Monte Carlo is described in Appendix C. All electromagnetic shower generation is done by the EGS4 code system. Propagation of through-going particles (pions, protons and cosmic ray muons) is done including the effects of dE/dx losses, multiple scattering and δ-ray production. Ray tracing of Čerenkov light is carried out for all charged particles above threshold for producing Čerenkov light. Each photon is propagated to a fate of either being absorbed, escaping the block or hitting the PMT. For the Čerenkov photons which hit the PMT, quantum efficiencies are used to simulate photoelectron production.

The Monte Carlo responses of each lead-glass block shape to 1 and 3 GeV incident electrons has been studied. The number of photoelectrons resulting from the Monte Carlo has been used with the PMT tests to set the initial operating voltages of the counters for the cosmic ray muon tests. The Monte Carlo responses of each shape to through-going cosmic ray muons and test beam pions and protons are discussed in the following sections as well as in Appendix C.

Figure 4.1: The cosmic ray muon test set-up and data acquisition with a counter in position. Distances are not shown to scale.

4.1.2 Cosmic Ray Test

After being assembled, each counter has been tested with through-going cosmic ray muons. The test was conducted with the counters oriented so that the phototube looked upward, as shown in figure 4.1. The average energy of a cosmic ray muon at sea level is approximately 2 GeV; through-going muons that intersect both the front and back faces of the block produce Čerenkov light initially directed towards the PMT. The amount of Čerenkov light collected by the counter's PMT is proportional to the particle's path length and the percentage of the block's back face covered by the PMT.

Twenty-four testing positions located in four dark boxes (each equipped with a patch panel for operating high voltage cables, signal cables and a fiber optic feed-through) allowed for several counters to be tested at the same time. Two scintillator paddles were associated with each testing position: above and below the counter. An upper scintillator paddle (2×3 in^2) was located 68.0 cm from the lead-glass PMT interface: 18.0 cm above the front face of any of the longest blocks. Located 31.1 cm below the lead-glass PMT interface was 4×4 in^2 scintillator paddle. A coincidence of the signals from the PMT's attached to the two scintillator paddles for a testing position formed the trigger for a through-going cosmic ray muon. The coincidence also ensured that the cosmic ray muon path traversed the entire length of the block. However for the smaller blocks, a triggered muon could miss the front face of the block. A small light source was sometimes on the front face of a counter during the test (see next section).

Each position was also equipped with a fiber optic cable (from a minor mixing bar connected to the fiber optic feed-through of the dark box) which was connected to the counter being tested. The spare flashlamp setup with major mixing bar of ten output fiber optic cables, of which four were connected to the dark boxes feed-throughs, provided light pulses to test the stability of the counters during the test run as well as test the gain monitoring system. The initial operating voltage for a counter was determined from the Monte Carlo of the shape and the PMT's gain curve parameters (section 3.2.1).

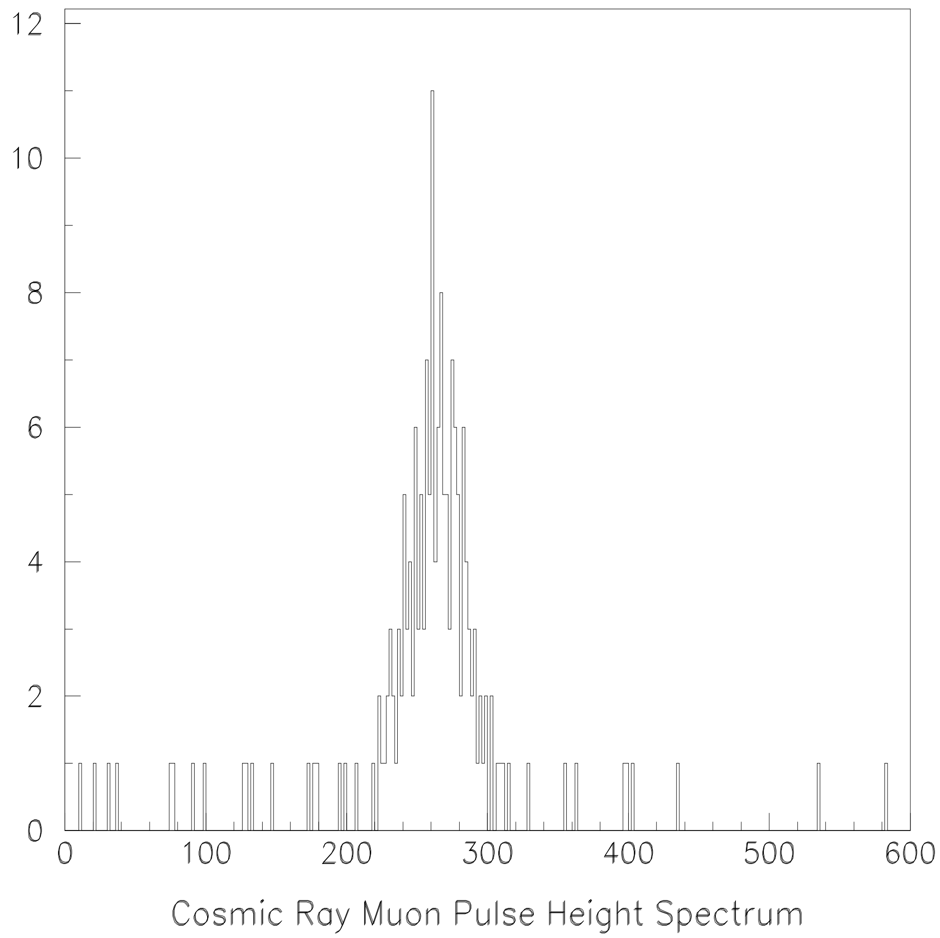

Figure 4.2: A typical spectrum of a counter's response to cosmic ray muons during the initial calibration and testing. Horizontal axis is ADC channel number.

Tests were conducted for twelve to sixteen hours with the flashlamp operating at $\frac{1}{6}$ Hz. The responses to the flashlamp and cosmic ray muons were triggered and recorded by a data acquisition and computer system. Over the course of a cosmic ray test run, each position would trigger upon approximately a thousand cosmic ray events. Figure 4.2 shows a counter's cosmic ray muon response spectrum; the response to the flashlamp system is shown in figure 4.3. The spectra from the flashlamp and cosmic ray muons were fit separately and recorded. The means of the cosmic ray

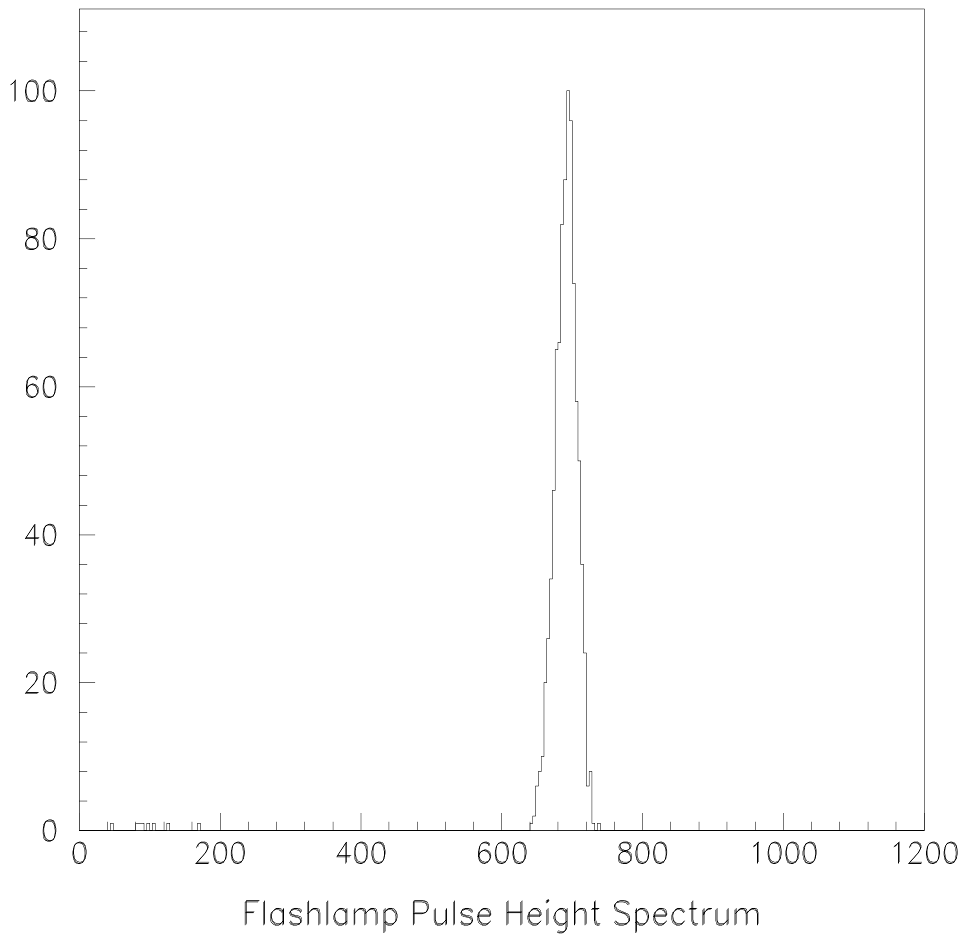

Figure 4.3: A typical spectrum of a counter's response to the flashlamp system during the cosmic ray muon tests. Horizontal axis is ADC channel number.

muon spectra are expected to be the same for all counters from the same ring and used to calibrate the counters with the same shape to have the same gain constant.

A Monte Carlo simulated response to cosmic ray muons was also performed. The Monte Carlo ratio of the expected number of photoelectrons from a 1 GeV incident e^- and a cosmic ray muon was used to further tune operating voltages for counters. The Monte Carlo showed the same distribution characteristics as the cosmic ray muon tests: a high energy tail due to light from δ-ray production and low energy tails for the smaller blocks due to the incident particles missing the front face.

4.2 Calibration with Particle Beams

Two electron test beams were used to examine a subset of the counters. Sixty counters, comprising three wedges, were examined at beam energies between 1 and 4 GeV. This test beam also included π^-, K^- and $\bar{p}$ particles which allowed study of through-going particles. A low energy test with an e^- beam of energy less than 100 MeV was performed upon five counters that were also tested at the higher energies.

The PMT gains were monitored at each particle beam test as well as during the cosmic ray tests. Attached to the front face of each counter was a ^{207}Bi–plastic scintillator light pulser. A Bi light pulser is cylindrical with a height of 1 cm and a diameter of 1 cm; the Bi is located between two pieces of scintillator. The pulser is a constant light source with the decay electron being contained within the scintillator sandwich. The pulser spectra, as shown in figure 4.4, provide a monitor of the PMT gains. As long as the Bi light pulser is attached to a counter, a known response could be measured independent of the setup.

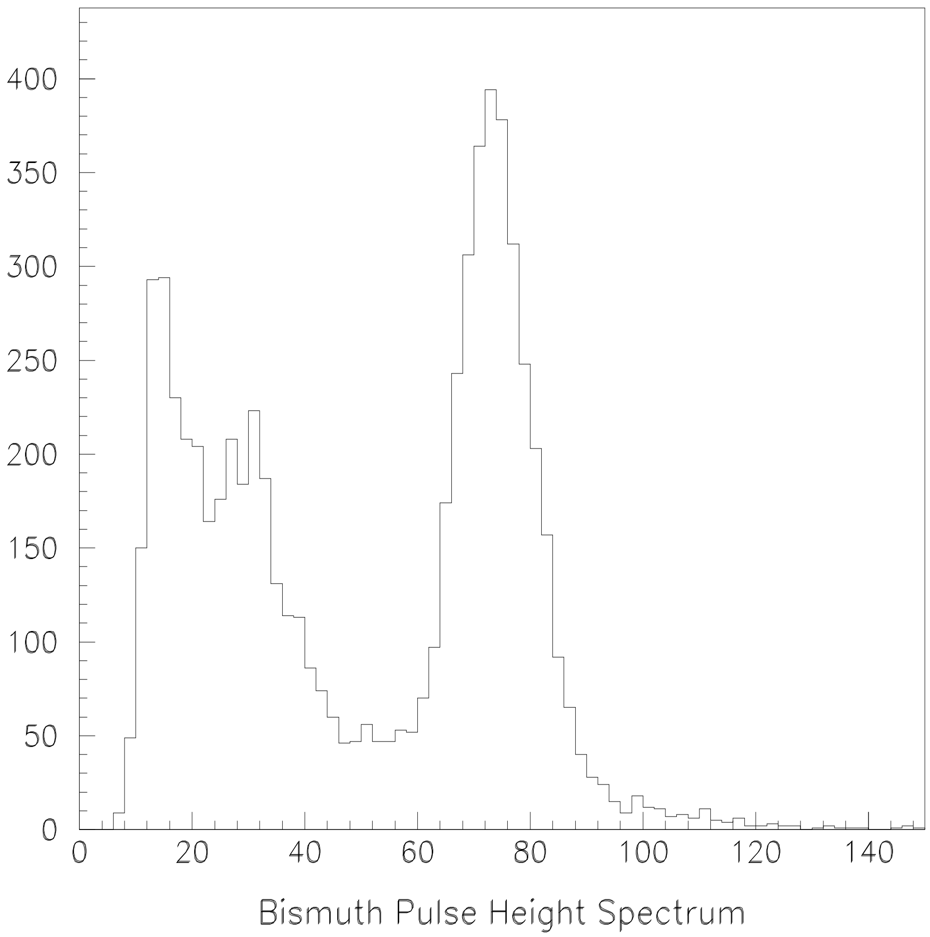

Figure 4.4: A typical spectrum of a counter's response to a Bi light pulser during the cosmic ray muon tests. Horizontal axis is ADC channel number.

4.2.1 High Energy Incident Particles

The equivalent of three wedges of the central calorimeter was studied at the Medium Energy Separated Beam (MESB-B2) of the Alternating Gradient Synchrotron (AGS) at Brookhaven National Laboratory. The MESB-B2 beam line is composed of negatively charged particles; the e^- component of the beam (2%) was tagged using a threshold Čerenkov counter. A trigger for the through-going π^-, K^- and $\bar{p}$ particles was also implemented using a setup of two scintillator paddles (10×10 mm^2 and 100×100 mm^2) similar in concept to the cosmic ray test.

The counters were supported on a horizontal test stand which had three degrees of freedom. The stand allowed for any of the sixty blocks in the three wedge configuration (prototype wedge shells were used) to be aligned with the beam. Two proportional wire chambers with 1 mm pitch and two scintillators (100×150 mm^2) were used to track the particles before the counters. The counters were studied at beam energies of 1, 2, 3 and 4 GeV with a spread of $\pm$ 0.8% ($\sigma(E)/E$). The beam energy was checked by time of flight measurements of e^-'s and $\bar{p}$'s.

The operating voltages were determined from the Monte Carlo simulations, PMT gain curves and the cosmic ray muon results. After studying the response to the e^- beam, the gains were changed so that the FERA ADC full scale corresponded to 6 GeV. With the new gains, the response to both e^-'s and the through-going particles were studied.

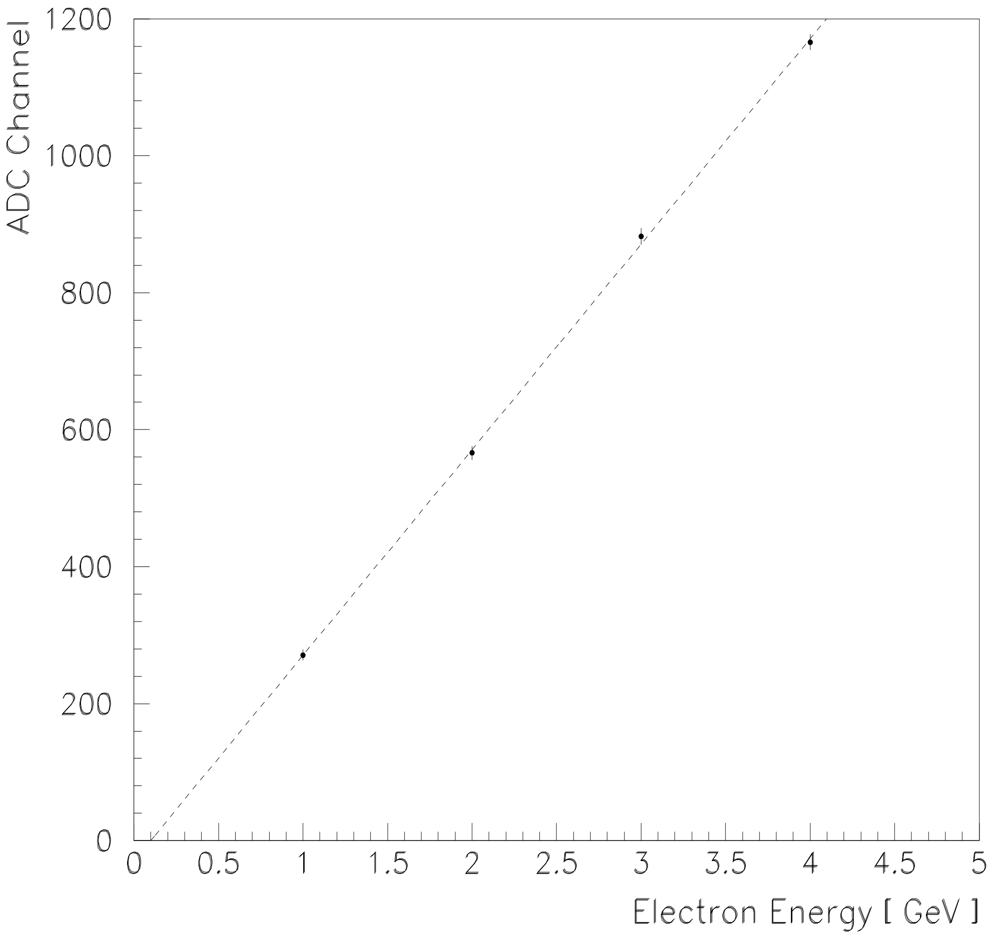

Figure 4.5: The linearity of response to electrons above 1 GeV.

The linearity of response to the four energies is shown in figure 4.5. Above 1 GeV it appears that the response is linear; the non-zero intercept means that the counters' responses at lower energies deviate from the linear response found at higher energies (see the next section and section 7.1). After unfolding the beam energy spread, the measured spread in energy for particles incident upon the center of counters from the middle wedge was found to be

$$\frac{\sigma(E)}{E} = \frac{(3.0 \pm 0.3)\%}{\sqrt{E}} + (1.5 \pm 0.5)\%, \tag{4.1}$$

where E is measured in GeV. The final energy resolution is given in section 7.1.

Since the relative calibration of counters within the same ring was being done with through-going cosmic ray muons, the through-going particles in the MESB-B2 beam line mentioned above were studied. The Monte Carlo showed a few percent difference between the responses of through-going cosmic ray muons with a range of incident angles with respect to the front face and beam particles normal to the front face. The ratio of responses of through-going particles and electrons was studied. Figure 4.6 shows the ratio of responses to incident π^-'s and incident e^- for the counters from the middle wedge for both the AGS and Monte Carlo data for 3 GeV incident particle energy. The electromagnetic shower width is comparable to the width of the larger numbered blocks. Therefore, the incident position is important for the amount of the shower contained within a single counter; the Monte Carlo assumes incident particles to hit the front face near its center. The summing of energy deposits into a 3×3 cluster of counters increases only the electron response. Figure 4.6 shows the ratio of responses for a cluster centered in the middle wedge for both the AGS and Monte Carlo data for 3 GeV incident particle energy. The Monte Carlo response is extrapolated from the response of the shape and a fictitious $30 \times 30 \times 50$ cm^3 lead-glass block (see Appendix C). The differences for the smaller blocks are explained by the material between the counters absorbing energy.

The three wedge configuration allowed for other studies. Electromagnetic shower energy sharing, energy loss due to the material in the cracks between counters and reconstruction of the incident particle track from the energy deposited were studied

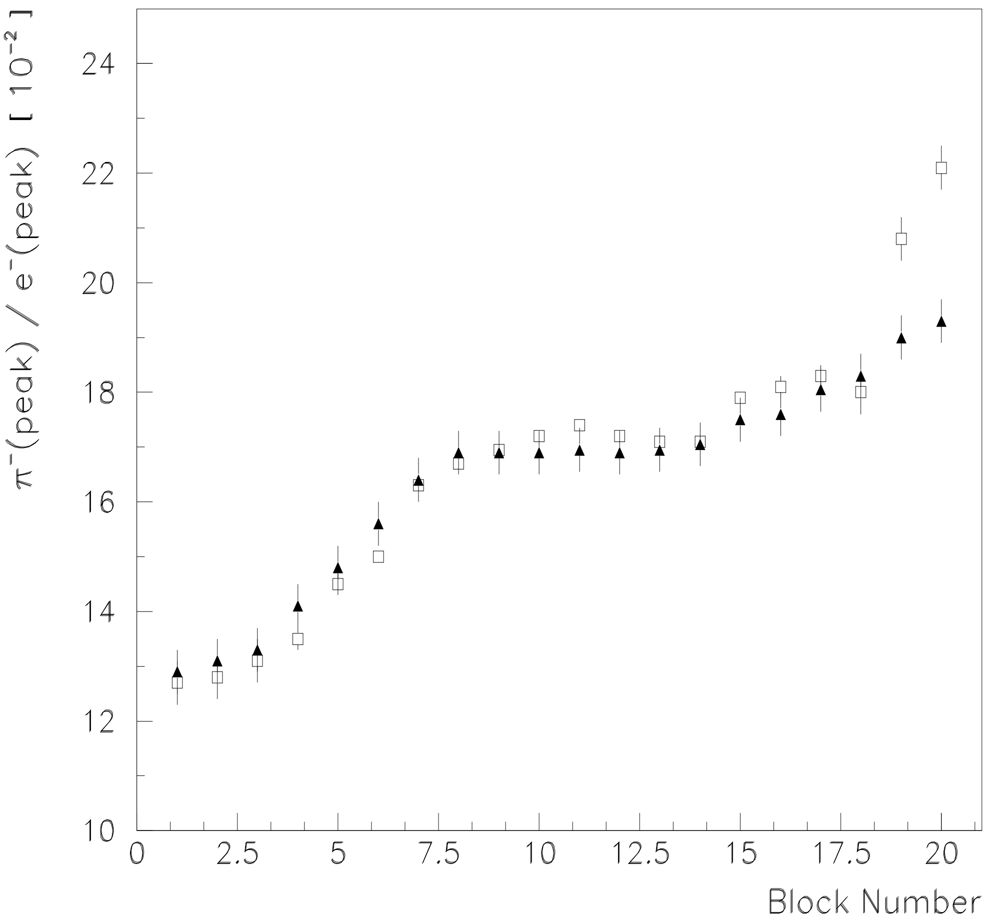

Figure 4.6: The ratio of responses to 3 GeV incident through-going π^- and electrons for individual counters from AGS data (squares) and Monte Carlo generated events (triangles).

as well as the degradation of the energy and position resolution as a function of how close an incident particle hits to a crack. Other tests involving single counters were done and are compared with the Monte Carlo simulations in Appendix C. Also a small target was inserted at approximately where the interaction region would be and the three wedge setup was able to reconstruct π^o's.

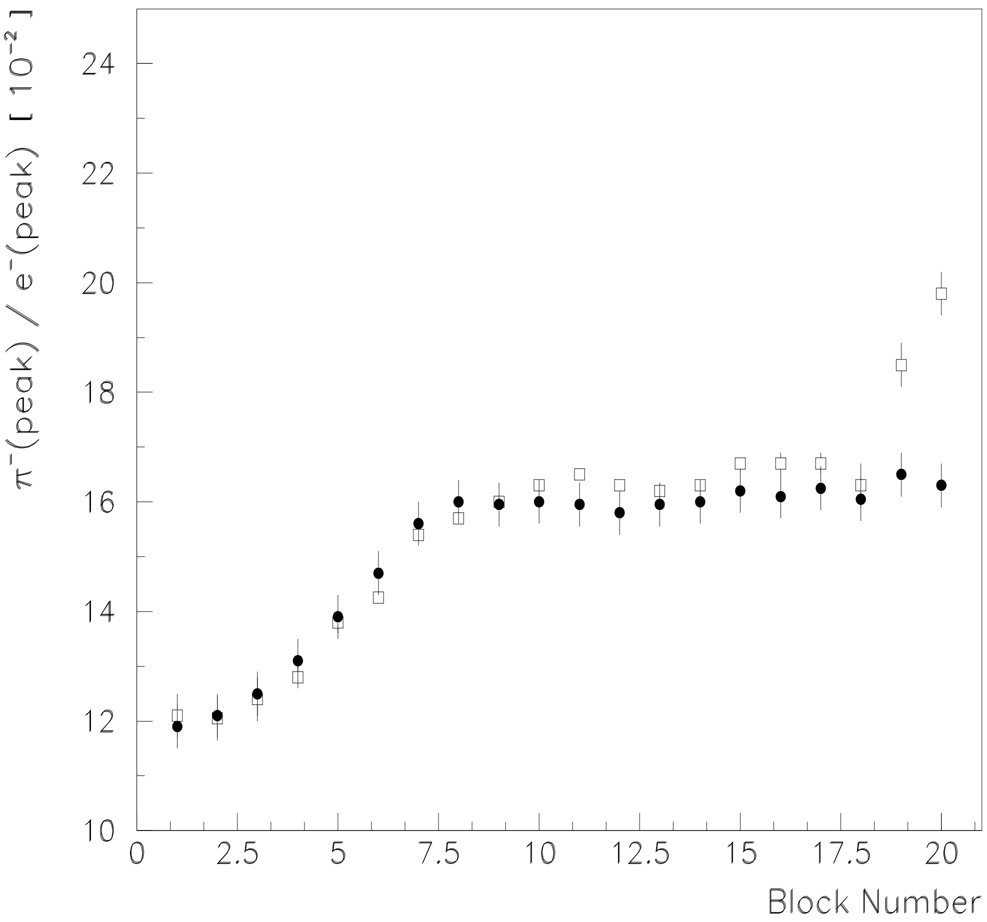

Figure 4.7: The ratio of responses to 3 GeV incident through-going π^- and electrons for a cluster from AGS data (squares) and Monte Carlo extrapolation (circles).

The summed signal was effectively increased by approximately 250 MeV when the incident particle went through the Bi light pulser; an even larger signal occurred when an incident e^- hit near one edge of a counter and then many electromagnetic shower particles escapes the initially hit block and went through the Bi light pulser of the neighboring counter due to the staggering of the blocks. It was determined that the pulsers affected the resolution too much and were removed from the counters after being re-tested in the cosmic ray setup with the new gains and prior to final installation of the counters into wedges. However, the known Bi light pulser response allowed for the calibration of the beam tested counters to be transferred as a calibration scale for the cosmic ray muon test.

4.2.2 Low Energy Incident Electrons

Five of the counters from the middle wedge tested at the AGS were also studied for low energy e^- response. The University of Illinois at Urbana Nuclear Physics Laboratory (UINPL) microtron provided a beam of 88 MeV e^-'s. Each counter was studied individually.

Each counter was placed at the correct angle inside a small dark box which aligned the counter's symmetry axis with the beam position and direction. A small scintillator paddle (10×10 mm^2) was placed in front of the small dark box opposite from the center of the front face of the block being tested. It was calculated that the beam energy was degraded to 84 MeV by passing through a target (from another experiment), an exit window, the scintillator paddle and one side of the dark box before hitting the counter.

The electron trigger was a coincidence of the signals from the counter and the PMT attached to the scintillator paddle. A qVt multichannel analyzer with a 160 ns external gate was used to collect the charge from the counter being tested. The Bi light pulser signal was close to the pedestal during the test at higher energies and the cosmic ray muon tests (figure 4.4); it was decided to operate the PMT's at a

Counter ID #	e^- Response	e^- FWHM/mean	Pulser Response
01-06	346	0.26	389
09-08	322	0.29	418
15-02	308	0.27	369
17-02	138	0.26	195
19-04	207	0.42	278

Table 4.1: The response to 84 MeV electrons and the light pulser; responses are the peak channel numbers.

higher voltage thus increasing the Bi light pulser signal a hundred channels above pedestal.

Table 4.1 shows responses to both the e^-'s and Bi light pulser at the microtron. The FWHM/mean of the 84 MeV electron response is included in table 4.1. The shape 19 counter tested is one of the smaller shapes which, as in the last section, means that the electromagnetic shower size is a big factor. The incident position affects how much of the shower is contained within the counter. Non-perfect counter alignment and electromagnetic shower particles escaping the shape 19 counter explain the significantly larger FWHM/mean.

The Bi light pulser *equivalent energy* was calculated assuming a linear response in the energy regime between 100 MeV to zero energy by

$$E_{eq} = \frac{R_{pulser}}{R_{e^-}} \times E_{e^-}. \tag{4.2}$$

Another equivalent energy for the Bi light pulser was calculated from the 3 GeV incident e^-'s of the high energy tests of the last section. The two equivalent energies

Counter ID	Equivalent Energy from 84 MeV e^-'s	Equivalent Energy from 3 GeV e^-'s	Calibration Error
01-06	94.4	84.8	−10.2%
09-08	109.0	94.9	−12.9%
15-02	100.6	91.8	− 8.7%
17-02	118.7	132.3	+12.3%
19-04	112.8	99.9	−11.4%

Table 4.2: The light pulsers equivalent energies calculated from responses to 84 MeV and 3 GeV electrons. The calibration error is from assuming a linear response to a counter calibrated at 3 GeV for a low energy incident electron.

are shown in table 4.2 along with the percentage error that would be made if linearity is assumed for the response using a calibration at 3 GeV for energies below 100 MeV.

Other tests were performed using the 84 MeV incident e^-'s. The responses of a counter operating with the voltage increased by 100 volts showed the expected mean increases from the previously determined PMT gain curves while not changing the FWHM/peak. Counter wrapping tests are compared with the Monte Carlo simulation in Appendix C.

4.3 Calibration with Data

The completed calorimeter's operating voltages were determined from the beam tests at high energies. The cosmic ray muon test allowed for the calibrations of the beam tested counter's to be transferred to the non-beam tested counters. The final calibration gain constants have been done in situ. Several methods have been tried to calibrate the calorimeter. The first methods discussed below are marginal due to statistics. The majority of the 1990 data was calibrated in this manner using data collected at the J/ψ energy. In 1991, a better method using $\bar{p}p \to \pi^o\pi^o$ was used to calibrate the calorimeter for every $\bar{p}$ stack. The calibration of the counters determined by the above methods of sections 4.1 and 4.2 was good to better than 20% and provided a good starting point for the methods described below.

4.3.1 $J/\psi \to e^+e^-$ Data

During 1990, the calibration was done for the counters in the rings numbered 1 to 15 with e^- and e^+ from J/ψ events. This calibration required that the experiment spend time acquiring e^- and e^+ at the J/ψ peak.

The e^- and e^+ energies can be determined kinematically by the polar angles measured by the tracking. The gains of the nine counters forming the 3×3 cluster defining an electron or a positron energy deposit were equally adjusted so that the measured summed signal was equal to the energy as determined kinematically by the polar angle. A counter's new gain would be the average of the adjustments from the entire J/ψ sample. The process was iterative; using new gains, the entire J/ψ sample was run again making new adjustments. The process was repeated until the difference in iterative gains was less than a few percent.

The number of times that each counter in the fifteen rings was hit directly varied between a few and a dozen. The statistics for any one counter was quite poor. A method of equalizing the gains from each counter was tried and is described in the next section. Kinematically, for both the e^- and e^+ to be within the acceptance of the central calorimeter, both had to be between rings 1 and 15; $\psi' \to e^+e^-$ extended the acceptance to ring 17 with much less statistics due to the smaller cross section. An attempt to *bootstrap* the calibration to the forward rings was tried and is discussed in section 4.3.3.

4.3.2 Punch Through Data

Signals from punch through particles from $\bar{p}p \to \pi^+\pi^-$ and elastic $\bar{p}p$ interactions have been used to try to calibrate the counters within a ring to have the same responses. A signal is defined to be a punch through particle when only one counter has a response; the Čerenkov light from a through-going particle should only be contained in one block. Assuming that the cosmic ray tests actually determined operating voltages, such that all the counters within the same ring had the same gain, the differences in the gains in the final experimental setup were caused by the full electronic readout. Using the punch through interactions, each counter's electronic channel could be adjusted to yield the same gain constant for counters in the same ring.

The interaction length, the hadronic equivalent of the radiation length, for the F2 lead-glass is 49 cm, approximately the length of most of the blocks. Therefore, it was expected that the probability of a punch through is e^{-1} per particle. However, due to the high rate of the hardware trigger for these events, the hardware trigger was prescaled (the trigger is discussed in Chapter 5). The number of punch through signals per counter is nearly the same number as of e^- or e^+ from the J/ψ events directly hitting a counter.

Each counter of a ring was normalized with the punch through signals and then the ring was considered as one object to be calibrated. The rings were then calibrated using the e^- or e^+ from the J/ψ events, thereby increasing the statistics. This combination process was not significantly better than using the $J/\psi \rightarrow e^+e^-$ events alone. If more punch through signals could have been recorded, this method might have proven to be better.

4.3.3 π^o Data

A bootstrap method of calibrating the counters of the forward rings used some of the many π^o's found in the data. Decays of π^o's were used when one gamma ray hit a forward counter and the other gamma ray hit a counter that was already calibrated by the methods described in the two previous sections. The invariant mass of the two clusters was used to adjust the gains of the uncalibrated counters in the forward rings; the gamma ray hitting a calibrated counter was considered perfectly measured.

As in the J/ψ data, the average adjustments were used to determine new gains and an iterative process was used. It was found best to do the iterative process one ring at a time. For instance, ring 16 counters would be calibrated with gamma rays hitting counters in this ring when the partner gamma rays were located in the previously calibrated counters of rings 1 to 15. When counters from ring 16 were considered calibrated, ring 17 counters were then calibrated. The process was iterated until the counters' calibration gain constants changed by no more than a few percent.

With the requirements of the partner gamma ray having a larger polar angle than the gamma ray being used to make the gain adjustment, and the opening angle of the π^o gamma rays large enough for the clusters to be separated, this method did a little better statistically. However, the errors of the gain constants for the forward counters were slightly larger than the errors of the gain constants determined for the other counters.

4.3.4 $\bar{p}p \rightarrow \pi^o\pi^o$ Data

The methods described in the previous three sections were used in 1990 to calibrate the calorimeter; calibration could only be performed whenever data was taken at the J/ψ energy (the π^o method of the last section required the J/ψ data for a starting point). The method used for the 1991 data allowed calibration to be performed on data taken every stack using $\bar{p}p \rightarrow \pi^o\pi^o$ events. These events are not prescaled and the gamma rays populated the entire calorimeter. Although the gamma rays nearly follow the $\pi^o\pi^o$ angular distribution, which is the same as the $\pi^+\pi^-$ distribution, the forward rings do get hit, not as often as the other rings.

When there are two sets of two clusters, with each set having an invariant mass roughly equal to the π^o mass, the direction of the π^o's are roughly determined. From the polar angle of a π^o, the energy of the π^o, and therefore the two gamma rays' total energy, is determined. This predicted energy is used to adjust the gain constants of counters involved forming both clusters. This method ignores the opening angle and treats overlapping clusters as one energy to be adjusted. The process is iterative. Three cluster events which satisfied the $\pi^o\pi^o$ hypothesis are also used. Other neutral two body reactions, $\pi^o\eta$ and $\eta\eta$, are used to check the calibration.

The $\bar{p}p \rightarrow \pi^o\pi^o$ method has been found to be superior to the previously used methods. The statistics of $\pi^o\pi^o$ events collected over an entire stack is sufficient to calculate gain constants for all of the calorimeter's counters.

4.4 Monitoring of the Calibration

In a sense, the best monitor of the calibration is the comparison of calibration gains as a function of time, i.e. for each stack. Two other methods, flashlamp gain monitoring and punch through particles, are used to monitor the gain constants and are discussed below. These methods also allowed monitoring of the radiation damage to the calorimeter.

4.4.1 Flashlamp Response

As described in the previous chapter, the response of each counter to the flashlamp was studied and recorded at each step during the construction and initial testing.

The flashlamp only provides a monitor and not a calibration since the flashlamp individual flashes vary in intensity and decrease slowly over time. The average flashlamp intensity seen by a counter is equivalent to a 1 to 2 GeV signal.

The flashlamp system was designed to study the calorimeter response over time to different parts of the Čerenkov light spectrum. The flashlamp system's filters allow monitoring different parts of the spectrum. Any counter's decrease in response to the flashlamp system can be caused by a decrease in flashlamp intensity, a malfunctioning photomultiplier tube or a yellowing of the lead glass due to radiation damage.

The flashlamp intensity is monitored by three phototubes. Three of the output fiber optic cables of the major mixing bar (section 3.1.5) are used to transport the flashlamp pulses to the phototubes. The responses of the three monitor phototubes are used to monitor the flashlamp intensity and normalize each flashlamp pulse. The monitor phototubes' stabilities are monitored by response to a Bi light pulser (section 4.2). The flashlamp intensity has slowly decreased over the course of data taking.

Malfunctioning photomultiplier tubes are identified by both flashlamp response and comparison of calculated gain constants every stack. Only two PMTs have failed and have been turned off. The flashlamp responses of these two PMTs did not differ from other counters before failure.

Radiation damage would be seen as a decrease of the response to the flashlamp by a large number of the calorimeter counters. No area of the calorimeter has been identified as having radiation damage. A discussion of radiation damage and curing of lead-glass blocks can be found in Appendix B.

4.4.2 Punch Through Particles

The punch through events are collected each stack and also provide a monitor. As with the attempt to calibrate with the punch through particles for the 1990 data, statistics for any counter for a stack is small due to the hardware prescale. However, over the course of several stacks the response of a counter to punch through particles can be used as a monitor.

Figure 4.8 shows the ADC channel spectra for two counters encompassing the entire 1991 data run. The mean channel numbers of the peaks are different since the counters are different lengths and have different percentages of the block's back face covered by the PMT. The low channel tail is from particles which interact in the counter and do not result in a large hadronic interaction (the signal is contained in the one counter). Figure 4.9 shows the same counters with the spectra corrected by each counter's gain constant (ADC channel $\times$ gain constant) resulting in *energy* spectra; note that the punch through signal is proportional to the charge particle path length and not the incident energy.

Figure 4.10 shows the ADC channel as a function of run number for punch through particles for one counter. Not all of the run numbers are represented; the density of data points is a function of the integrated luminosity per run, E_{cm} and

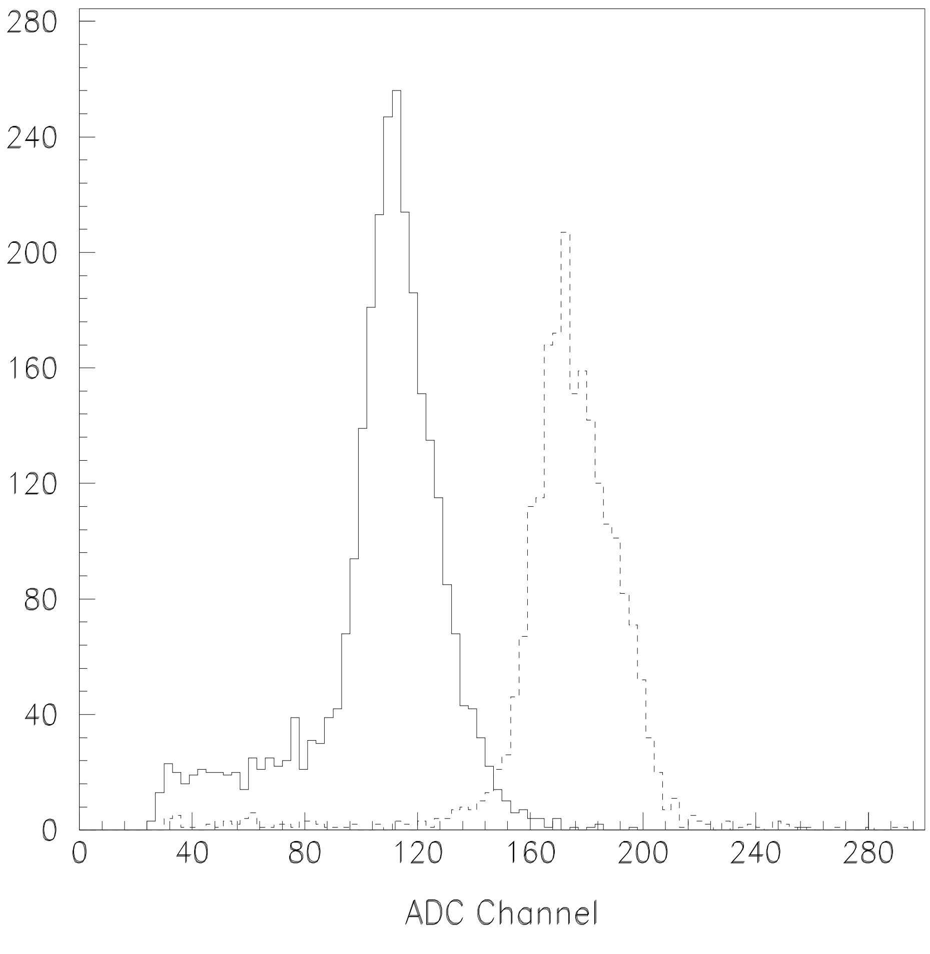

Figure 4.8: The ADC channel spectra for two counters' responses to punch through particles. The difference in mean channel is due to the different counter lengths and the percentage of the block's back face covered by the PMT.

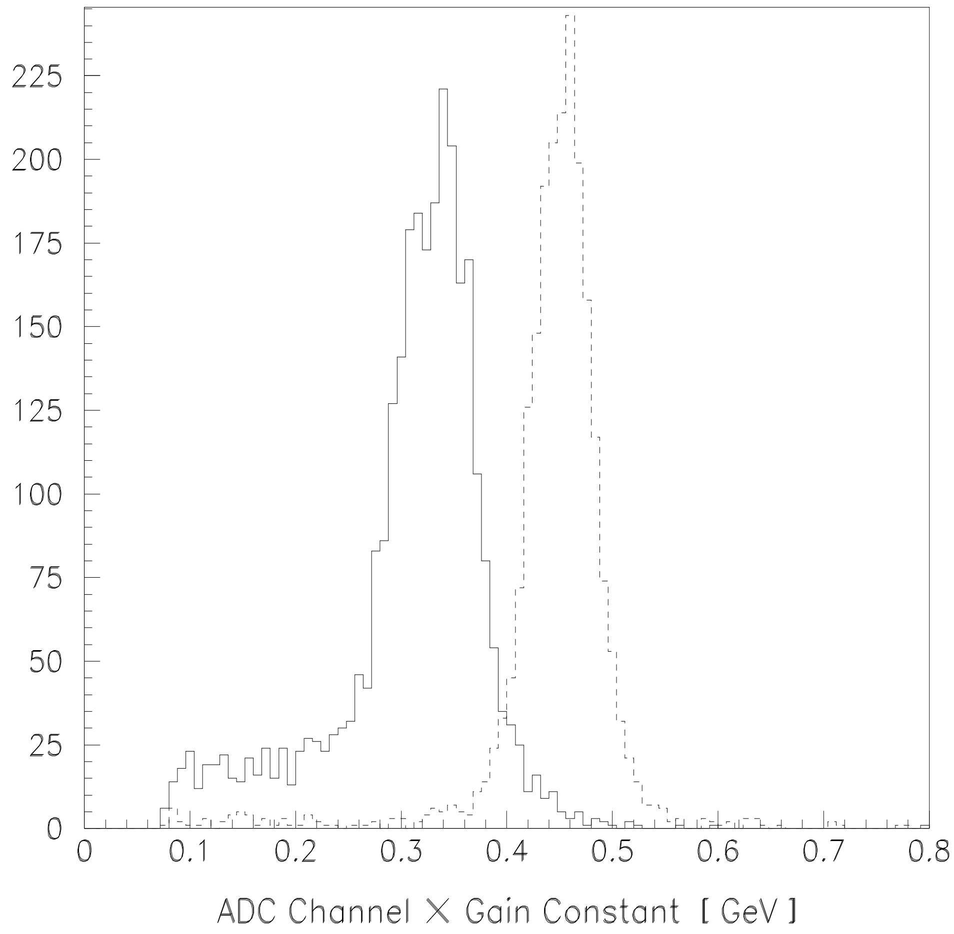

Figure 4.9: Two counters' spectra of the ADC channel multiplied by the counter's gain constant for punch through particles. The difference in mean value is due to the different counter lengths and the percentage of the block's back face covered by the PMT.

hardware prescale factor. The apparent discontinuity, drop in ADC level, at Run 1441 is from a change of the operating voltage. The nominal full scale FERA ADC energy equivalent is 5 GeV: a nominal gain constant of 2.6415 MeV/(ADC channel). The calibration gain constants prior to Run 1441 and the PMT gain curves were used to adjust the operating voltages so that all counters would have the nominal gain constant. Figure 4.11 shows the punch through particles *energies* as a function of run for the same counter. The resultant punch through signals show that the gain constants have been consistent for the entire 1991 data taking period.

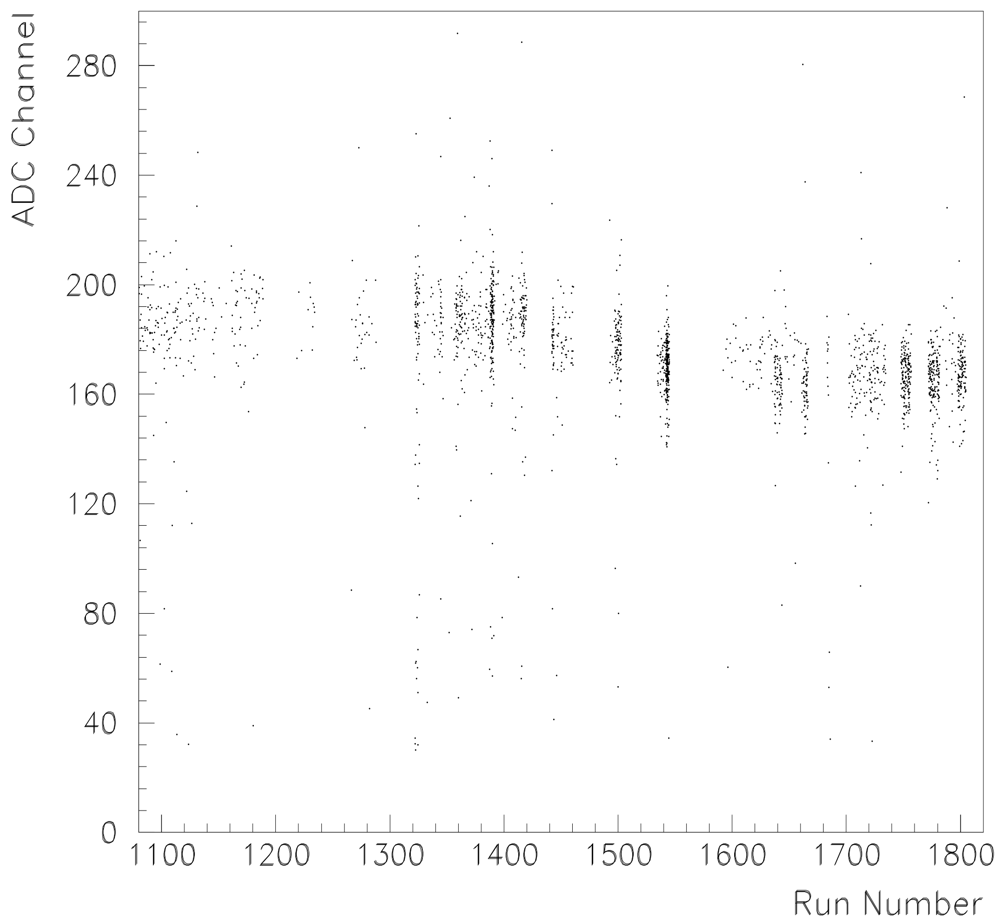

Figure 4.10: The ADC channel punch through response for one of the counters as a function of run number.

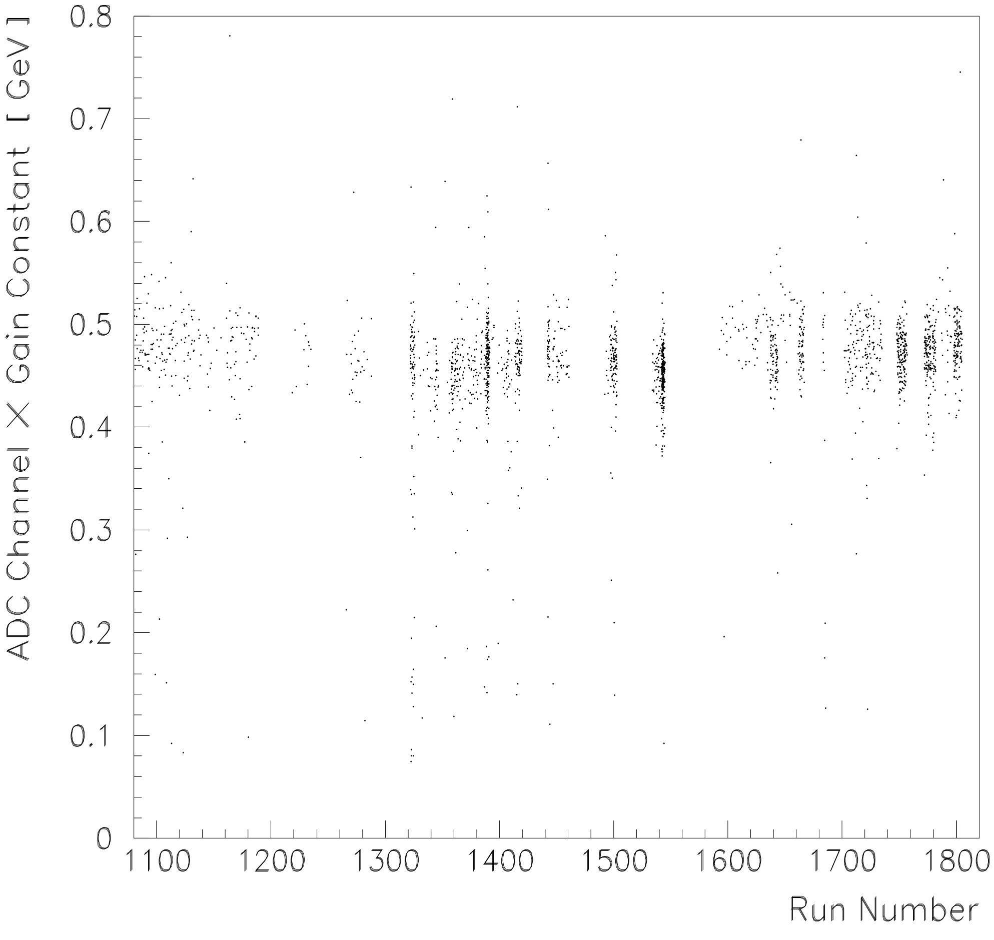

Figure 4.11: The ADC channel punch through response multiplied by the gain constant for one of the counters as a function of run number.